Carbohydrate Polymers 85 (2011) 129–137

Contents lists available at ScienceDirect

Carbohydrate Polymers

journal homepage: www.elsevier.com/locate/carbpol

Fabrication of UV-crosslinked chitosan scaffolds with conjugation of RGD peptides for bone tissue engineering

Wei-Bor Tsai [a,*], Yi-Ru Chen [a,b], Hsuan-Liang Liu [b], Juin-Yih Lai [c]

[a] Department of Chemical Engineering, National Taiwan University, No. 1, Roosevelt Rd., Sec. 4, Taipei 106, Taiwan
[b] Graduate Institute of Biotechnology and Department of Chemical Engineering and Biotechnology, National Taipei University of Technology, No. 1 Sec. 3 ZhongXiao E. Rd., Taipei 106, Taiwan
[c] R&D Center for Membrane Technology and Department of Chemical Engineering, Chung Yuan Christian University, Chungli, Taoyuan, Taiwan

ARTICLE INFO

Article history:
Received 16 November 2010
Received in revised form 27 January 2011
Accepted 1 February 2011
Available online 2 March 2011

Keywords:
Chitosan
Scaffolds
Osteoblasts
RGD
UV-crosslinking

ABSTRACT

In this study, a simple process was established to fabricate RGD-conjugated and crosslinked chitosan scaffolds for bone tissue engineering. Two types of chitosan derivatives were synthesized: one containing photoreactive azido groups and the other tethered with RGD. Their mixture was fabricated into chitosan scaffolds by freeze-drying and UV crosslinking. The pore size and mechanical property of the chitosan scaffolds were increased by 1.36 and 2.41 folds, respectively, by the post-crosslinking process. Incorporation of RGD enhanced the culture of the rat primary osteoblasts. After 10 days of culture, the cell number in the RGD-contained chitosan scaffolds was increased by 50% compared to the control. Furthermore, the calcium deposition by the osteoblasts in the RGD-incorporated chitosan scaffolds was almost doubled compared to the control, and thus greatly increased the mechanical property of the chitosan scaffolds. Our technique is proved useful in preparing scaffolds for bone tissue engineering and other biomedical applications.

1. Introduction

Chitosan, the deacetylated derivative of chitin, has been widely utilized in medical applications such as tissue engineering and wound repair (Muzzarelli, 2009a, 2011). Due to its biodegradability, good biocompatibility (VandeVord et al., 2002) and relatively better mechanical properties compared to some natural polymers (Majima et al., 2005), chitosan is a popular material for fabricating tissue engineering scaffolds, which allow cells to accommodate, grow, migrate and organize to form a functional tissue. Nevertheless, chitosan still possesses some shortcomings for scaffold fabrication. First, the mechanical property of chitosan scaffolds may not be sufficient to match some specific tissue engineering applications. Secondly, chitosan lacks bioactive signals existing in the extracellular matrix (ECM) for cell attachment, growth and differentiation. The above problems can be overcome by chemical crosslinking to improve the mechanical properties of chitosan scaffolds, and incorporation of bioactive molecules into chitosan scaffolds to enhance cell affinity. Some frequently used crosslinkers, such as glutaraldehyde and genipin, form covalent bonds with the amino groups of chitosan so as to increase the mechanical strength of chitosan scaffolds (Hoffmann, Seitz, Mencke, Kokott, & Ziegler, 2009; Hsieh et al., 2007; Kuo & Lin, 2006; Muzzarelli, 2009b).

Bioactive molecules used to enhance biomaterials' cellular affinity are usually derived from the ECM macromolecules. Cells in native tissues adhere to the surrounding ECM via cell membrane receptors (e.g. integrins Hynes, 1992) that specifically bind to ECM adhesion proteins such as collagen, fibronectin and laminin. One approach to improve biocompatibility of chitosan scaffolds is the incorporation of ECM proteins such as gelatine (Huang, Onyeri, Siewe, Moshfeghian, & Madihally, 2005; Wang, Chow, Lai, Liu, & Tsai, 2009). Alternatively, the conjugation of peptides containing cell-binding sequences of the ECM adhesion proteins also supports cell adhesion. The advantages of peptides include cost effectiveness and less vulnerability to denaturation in comparison with intact adhesion proteins. The most commonly applied cell-binding peptide is arginine–glycine–aspartic acid (RGD), which is found in ECM adhesion proteins such as fibronectin and laminin (Massia & Hubbell, 1990; Ruoslahti & Pierschbacher, 1987). Immobilization of RGD on chitosan molecules to enhance chitosan's cellular affinity has been demonstrated on two-dimensional film structures (Chung, Lu, Wang, Lin, & Chu, 2002; Hacker et al., 2003), but rarely in three-dimensional scaffolds. Previously, Ho et al. (2005) conjugated RGDS peptides onto chitosan scaffolds by an imide-bond forming reaction between the amino groups of chitosan and the carboxyl groups in RGD peptides. They showed that RGDS-immobilization

* Corresponding author. Tel.: +886 2 3366 3996; fax: +886 2 2362 3040.
E-mail addresses: weibortsai@ntu.edu.tw (W.-B. Tsai), med403@gmail.com (Y.-R. Chen), f10894@ntut.edu.tw (H.-L. Liu), jylai@cycu.edu.tw (J.-Y. Lai).

0144-8617/$ – see front matter © 2011 Elsevier Ltd. All rights reserved.
doi:10.1016/j.carbpol.2011.02.003

enhanced the proliferation of the osteoblast-like cells and mineral deposition in the chitosan scaffolds.

Although RGD-conjugation and crosslinking of chitosan scaffolds are frequently found in the literature, it is hardly found a facile protocol for simultaneous crosslinking chitosan scaffolds and conjugating RGD peptides. The reason might be due to that both reactions usually interfere with each other since they often utilize the amino groups of chitosan. Azide chemistry, which has been used for preparation of crosslinked chitosan hydrogels for wound dressing and cell culture (Fukuda et al., 2006; Karp et al., 2006; Obara et al., 2003), might be applied for simultaneous crosslinking chitosan scaffolds and conjugating RGD peptides. The biocompatibility of azides as photocrosslinkers has been previously demonstrated (Ishihara et al., 2002; Obara et al., 2003; Ono et al., 2000). This study was aimed to develop a facile and reliable method to fabricate RGD-containing chitosan scaffolds with controllable mechanical properties by azide chemistry. The application of the RGD-containing crosslinked chitosan scaffolds to bone tissue engineering was also evaluated.

2. Materials and methods

2.1. Materials

Most of the reagents were purchased from Sigma–Aldrich (USA) unless specified otherwise. *N*-(3-dimethylaminopropyl)-*N*′-ethylcarbodiimide hydrochloride was purchased from Fluka (USA). Osteoblast culture medium contained α-minimum essential medium (α-MEM, HyClone, USA), 10% fetal bovine serum (JRH Biosciences, Australia), 0.0679% (v/v) 2-mercaptoethanol, 200 μg/mL gentamicin (GIBCO®, Invitrogen, USA) and 25 μg/mL fungizone (GIBCO®), pH 7.4. The osteoblast culture medium supplemented with 1 mM sodium glycerophosphate, 0.1 μM dexamethasone and 50 μg/mL L-ascorbate constituted osteoblast differentiation medium. Phosphate buffered saline (PBS) contained 137 mM NaCl, 2.7 mM KCl, 10 mM Na_2HPO_4, and 1.8 mM KH_2PO_4 (pH 7.4), and was sterilized by autoclave.

RGD-peptide (*N*-acetyl-G**RGD**SPGYG-amide) was synthesized by Kelowna International Scientific Inc. (Taipei, Taiwan). Peptide concentration was calculated by absorbance at 275 nm coming from tyrosine residue (Y, molar adsorption coefficient 1420 M^{-1} cm^{-1}).

2.2. Conjugation of photoreactive azido groups or peptides onto chitosan molecules

Photoreactive azido groups were conjugated onto chitosan (molecular weight 50–190 kDa, 75–85% deacetylation) via a reaction forming covalent imine bonds between the amino groups of chitosan and N-hydroxysuccinimide moiety of 5-azido-2-nitrobenzoic acid N-hydroxysuccinimide ester. Briefly, 17.6 mg 5-azido-2-nitrobenzoic acid N-hydroxysuccinimide ester was dissolved in 200 μL dimethylsulfoxide and then mixed with chitosan solution (0.1 g in 4.8 mL of 1% acetic acid), followed by 3 h incubation at room temperature. The unreacted azido ester was removed by dialysis against deionized water through a seamless cellulose tube (MWCO 12,400) in the dark for two days with changes of deionized water every 12 h. After freeze-drying, the azido-conjugated chitosan (azido-chitosan) was kept at 4 °C until use.

The content of azido groups in azido-chitosan was determined by ^1H nuclear magnetic resonance (^1H-NMR, Avance-500 MHz, Bruker). The ^1H NMR spectrum of the unmodified chitosan (1 wt% in 1% CD_3COOD/D_2O, see supplement S1) was similar to a previous report (Hirai, Odani, & Nakajima, 1991). In the ^1H NMR spectrum of azido-chitosan, the peaks appearing around chemical shifts 6.84–8 ppm represented the aromatic protons of the azidobenzoic groups (see supplement S1). The coupling percentage of the azido groups in azido-chitosan was estimated at 3.9 mol% of the amino groups of chitosan, according to the ratio of the peak areas of the aromatic protons to the –C<u>H</u>–NH_2 proton (H_b) at 2.86 ppm.

Table 1
The weight percentages of the compositions in the chitosan mixture for films or scaffolds. The total concentration for all the chitosan mixture is 10 mg/mL in 1% acetic acid.

Abbreviations for films or scaffolds	Chitosan (%)	Azido-chitosan (%)	Chitosan-g-RGD (%)
CHITOSON	100	0	0
c-CHITOSAN-10	90	10	0
c-CHITOSAN-30	70	30	0
c-CHITOSAN(-50)[a]	50	50	0
c-CHITOSAN-RGD[b]	46	50	4

[a] For cell culture experiments, the concentration of azido-chitosan was fixed at 50%, so "50" was omitted in the abbreviations.
[b] The RGD contents in the c-CHITOSAN-RGD scaffolds were estimated as 0.63 μmole/scaffold.

RGD peptides were conjugated onto chitosan molecules via a carbodiimide reaction. Briefly, 16 mg RGD-peptide (0.017 mmol), 3.6 mg *N*-(3-dimethylaminopropyl)-*N*′-ethylcarbodiimide hydrochloride (0.017 mmol) and 1.9 mg N-hydroxy-2,5-pyrrolidinedione (0.017 mmol) were dissolved in 60 μL N, N-dimethylformamide and then mixed with 3 mL of chitosan solution (2%, w/v in 1% acetic acid). After 24-h incubation at room temperature, the mixture was dialyzed against deionized water. After freeze-drying, the peptide-grafted chitosan (chitosan-g-RGD) was stored at −20 °C until use. The graft ratio of RGD to chitosan was estimated as 2.75 mol% with respect to the total moles of the amino groups of chitosan molecules.

2.3. Preparation of the chitosan films and scaffolds

Chitosan films were prepared by adding mixture of chitosan, azido-chitosan and chitosan-g-RGD in different ratios (listed in Table 1) into 96-well TCPS plates (70 μL/well). The chitosan solution was then allowed to dry in the air at room temperature. The dried chitosan films were subjected to UV irradiation for 30 min at 12 cm below a halogen UV lamp (wavelength range 280–380 nm). The light intensity at this distance was determined as 65 mW/cm^2 by a UV radiometer.

Chitosan scaffolds were prepared by the freeze-drying technique, which is widely applied to fabrication of porous chitosan scaffolds (Ho et al., 2004; Madihally & Matthew, 1999). The chitosan mixture with different compositions (the compositions and the abbreviations listed in Table 1) was poured into 96-well TCPS plates (70 μL/well for cell culture experiments and 336 μL/well for mechanical testing), followed by freeze-drying/crosslinking processes.

2.4. Characterization of the chitosan scaffolds

The porous structure of the chitosan scaffolds was observed by scanning electron microscopy (SEM, JSM-5310, JEOL, Japan). The scaffolds were first dehydrated in a graded series of ethanol solutions: 30%, 50%, 70%, 90%, 95%, 100% for 10 min for each step, followed by CO_2 critical point drying. After subjected to gold sputtering, the samples were observed using SEM with an acceleration voltage of 20 keV.

The pore sizes of chitosan scaffolds were analyzed from the SEM images by using NIH Image J. The pores were traced manually in SEM images and the enclosed areas and the perimeters of pores were determined by Image J. The hydraulic diameters of the pores were determined by the following equation: pore diameter

(D_p) = 4 × area/perimeter (Innocentini, Salvini, Pandolfelli, & Coury, 1999). More than 100 pores were counted for each type of the samples.

The compressive stress–strain property of the chitosan scaffolds was determined using a compressive testing machine (FGS-50V-H, NIDECSIMPO Corporation, Japan) and a digital force gauge (FGP-0.5, NIDECSIMPO Corporation, Japan). Prior to the mechanical compression test, the chitosan scaffolds were trimmed to approximate 5 mm thick. Dried scaffolds were rehydrated in PBS (pH 7.4) at room temperature for 1 h prior to the mechanical testing. The chitosan scaffolds were subjected to an unconfined uniaxial compression to 95% strain at a compression velocity of 2 mm/s, followed by relaxation testing.

2.5. Cell culture

Standard sterile cell culture techniques were used for all cell experiments. Primary osteoblasts were isolated from neonatal rat calvariae according to a previous procedure (Bakker & Klein-Nulend, 2003). The number and viability of the isolated cells were determined using a hemocytometer with trypan blue exclusion. Almost all the isolated cells were identified as osteoblasts by an alkaline phosphatase staining method as reported previously (Tsai et al., 2009). The isolated osteoblasts were cultured in standard T75 flasks to the second passage for the cell experiments.

Prior to cell seeding, the chitosan samples were soaked in 70% ethanol for 30 min, followed by three rinses with sterilized PBS. For cell culture on the chitosan films, the cells suspended in the osteoblast culture medium (8×10^4 cells/mL) was added onto the chitosan films (50 μL/well), making the seeding density as 1.25×10^4 cells per sample area (cm^2). After 1, 5 or 10 days of culture, the cell morphology was observed under a phase contrast microscope and the cell numbers were determined. For the cell culture in the chitosan scaffolds, 50 μL of the osteoblast suspension (6×10^6 cells/mL) was inoculated into the chitosan scaffolds, making the seeding density as 3×10^5 cells per scaffold. After 1, 5 or 10 days of culture, the cell-seeded samples were analyzed.

The cell numbers on the chitosan films or scaffolds were determined by a lactate dehydrogenease assay, which was modified from a previous procedure (Tsai, Shi, Grunkemeier, McFarland, & Horbett, 2004) and reported previously (Tsai, Chen, Wei, Tan, & Lai, 2010). Briefly, the attached cells were lysed with 1% Triton X-100 in PBS, and 50 μL of the supernatant of the cell lysates after centrifugation at 1000 rpm was mixed with 60 μL of the reaction solution (3.6% sodium lactate, 0.3% NAD^+, 0.27% diaphorase, 0.03% bovine serum albumin, 1.2% sucrose, and 0.02% indonitrotetrazolium in deionized water). The reaction was undergone at 37 °C in the dark and then stopped by adding 20 μL of 1.6% sodium oxamate. The optical densities at 490 nm were read with a microtiter plate reader (Bio-Tek, EL800, USA). A standard plot was generated with a series of cell lysates with known cell densities.

Intracellular alkaline phosphatase activities were assayed by determining the release of *p*-nitrophenol from 4-nitrophenyl phosphate disodium salt at pH 10.2, as reported previously (Tsai et al., 2009).

2.6. Mineralization culture of the osteoblasts/scaffold constructs

The osteoblast/scaffold constructs were cultured for 10 days in the osteoblast culture medium, followed by 15-day mineralization culture in the osteoblast differentiation medium with daily replenishment of freshly prepared L-ascorbate (50 μg/mL). The total amount of calcium deposition was determined using a calcium assay kit (Diagnostic Chemicals Limited, USA) according to a previous protocol (Tsai et al., 2010).

For histological analysis, the cell/scaffold constructs were fixed in 4% formaldehyde, and then dehydrated in a graded series of ethanol solutions. The constructs were soaked in xylene and then embedded in paraffin. The paraffin blocks were dissected into 6 μm-thick sections by microtome incision. After removal of paraffin by soaking in xylene and then rehydration of the samples, the slides were then stained with Alizarin red S solution (pH 5.5) at room temperature for 20 min. After rinsed with deionized water, the stained samples were observed under a light microscope.

2.7. Statistics

Each experiment has been repeated at least three times. Statistical assessment of significant variations was performed by GraphPad Instat® 3.00 (GraphPad Software Inc.). Significance was assessed by one way analysis of variance (ANOVA) and two-tailed Student–Newman–Keuls multiple comparison.

3. Results and discussion

3.1. Fabrication of the UV-crosslinked chitosan scaffolds

The azide-based UV-crosslinking mechanism was used for crosslinking the chitosan scaffolds in this study. Upon UV irradiation, the azido groups are converted into highly reactive nitrene groups and release N_2 gas. The nitrene groups ought to be undergone direct insertion into C–H, O–H, and N–H bonds of nearby substance molecules (Das & Fox, 1979). Two different freeze-drying/crosslinking processes were evaluated in this study. The first type of scaffold fabrication started with exposure of chitosan solutions to UV for 30 min, followed by freezing at −20 °C overnight and then freeze-drying. The crosslinked chitosan scaffolds formed in this process were referred as "pre-crosslinking". The second process, in contrast to the former one, began from freeze-drying of chitosan solution in the dark to form scaffolds, followed by 30-min UV irradiation. This type of chitosan scaffolds was referred as "post-crosslinking".

We first evaluated the effects of the contents of azido-chitosan in the chitosan scaffolds on the morphology and mechanical properties. The microscopic morphology of both classes of the chitosan scaffolds, i.e. pre-crosslinking and post-crosslinking, exhibited an open and inter-connective porous microstructure (Fig. 1A). No obvious discrepancy in the pore structures was observed among the different types of the chitosan scaffolds. Quantified data indicated that the average pore diameters of the pre-crosslinking chitosan scaffolds were slightly increased with the azido-chitosan contents, which is similar to a previous report by Ling et al. (2008). However, the sizes were all around 110 μm, comparable with the unmodified chitosan scaffolds ($p > 0.05$, Fig. 1B). On the other hand, the average pore sizes of the post-crosslinking chitosan scaffolds were significantly increased with increasing azido-chitosan contents, from 110.1, 131.7 to 149.4 μm for the post-crosslinking samples containing10%, 30% and 50% azido-chitosan, respectively. The average pore size of the post-crosslinking c-CHITOSAN-50 samples was significantly larger than those of the other scaffolds ($p < 0.001$).

We suspect that the increase in pore sizes with the contents of azido-chitosan may occur at the phase-separation stage during freezing, although Ling et al. (2008) conjectured that the increase in pore sizes is due to the released N_2 bubbles acting as porogen. During the freezing process, phase separation (so-called solid–liquid de-mixing) of chitosan solution occurs, leading to the formation of solvent-rich domains and chitosan-rich domains (Ho et al., 2004). After sublimation of frozen solvent, the solvent-rich domains form the porous structures of chitosan scaffolds. Therefore, porous structures are mainly determined by the formation

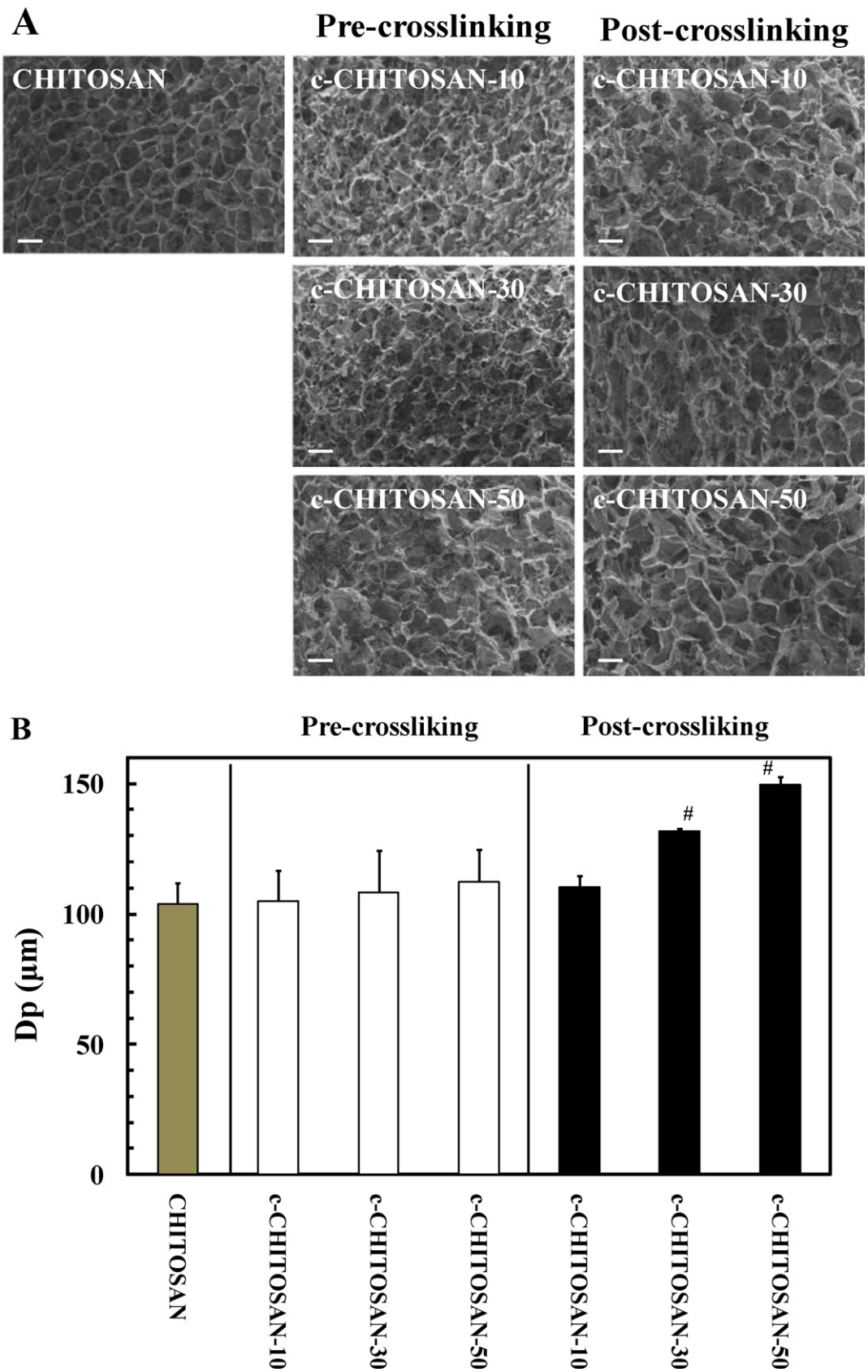

Fig. 1. (A) The SEM images of the chitosan-based scaffolds. Scale bar = 100 μm. (B) The average pore diameter (D_p, μm) of the chitosan-based scaffolds. The data are presented as mean ± standard error of the mean, $n = 100$. #, $p < 0.001$ vs. the other types of the chitosan-based scaffolds.

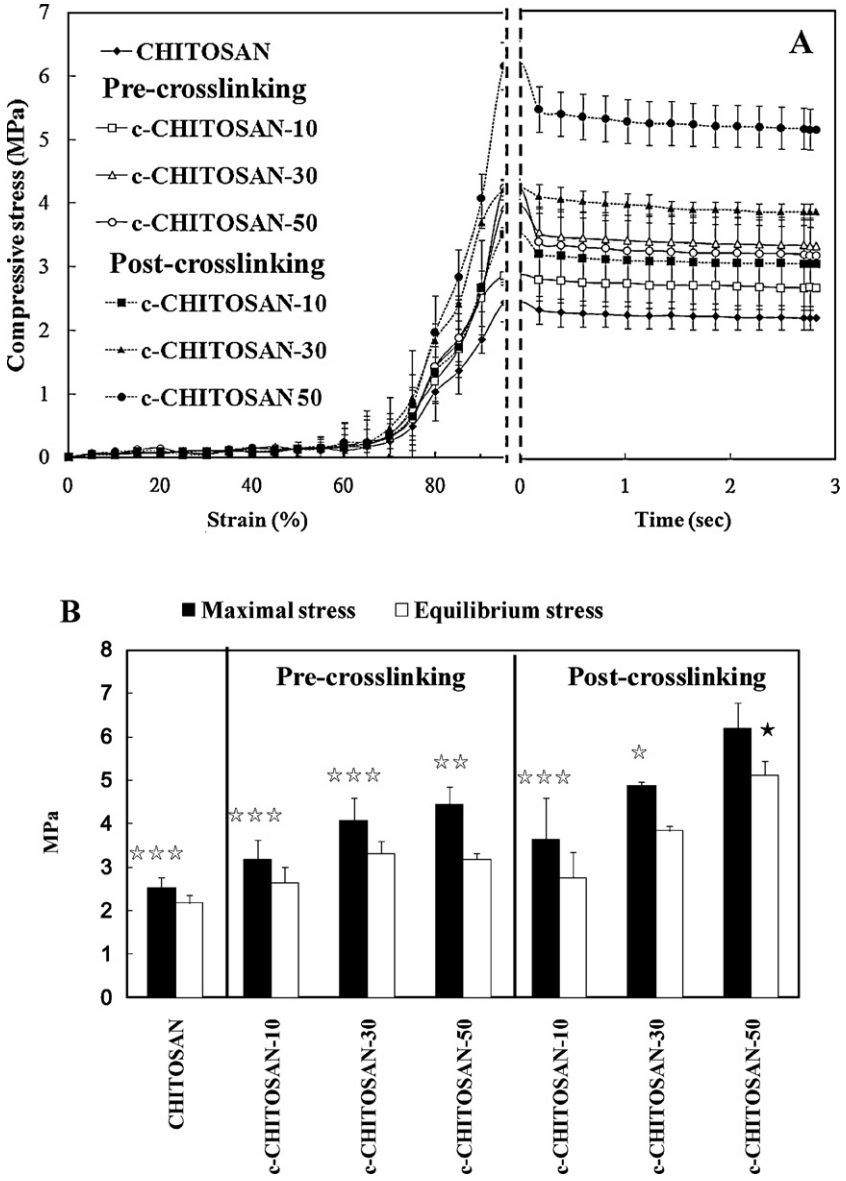

Fig. 2. (A) The left side of the plot represents the compressive stresses of various chitosan scaffolds against the compressive strain. The right side of the plot represents the changes in the compressive stresses of the chitosan scaffolds during the relaxation testing. The data are presented as mean ± standard error of the mean, $n = 4$. (B) The maximal compressive stresses of the chitosan scaffolds at 95% strain and the equilibrium stresses after relaxation. The data are presented as mean ± standard error of the mean, $n = 4$. ☆, ☆☆ and ☆☆☆ represent $p < 0.05$, 0.01 and 0.001, respectively, vs. the maximal stress of post-crosslinking c-CHITOSAN-50. ⋆ represents $p < 0.001$ vs. the equilibrium stresses of the other scaffolds.

of the solvent-rich domains during the phase-separation stage. The hydrophobic azido moiety of azido-chitosan may enhance the segregation of the solvent-rich domains and the chitosan-rich domains. Therefore, larger solvent-rich domains form in the presence of azido molecules, resulting in an increase in the pore sizes in accordance with the contents of azido-chitosan in the post-crosslinking process.

The compressive properties of the chitosan scaffolds were next evaluated (Fig. 2A). The compressive stresses of all the chitosan scaffolds remained low until 65% strain compression, and increased with increasing strain until a maximum at the end of compression (95% strain). The maximal compressive stresses of the crosslinked scaffolds were higher than the un-crosslinked one, indicating that the stiffness of the chitosan scaffolds was enhanced by UV-crosslinking. Furthermore, the compressive strain was increased in accordance with the contents of azido-chitosan (Fig. 2B). Compared to the maximal compressive stress of the unmodified chitosan scaffolds (2.57 ± 0.52 MPa), those of pre-crosslinking scaffolds were increased from 3.17 ± 0.42, 4.08 ± 0.51 to 4.44 ± 0.39 MPa for 10%, 30% and 50% azido-chitosan samples, respectively. The post-crosslinking process increased the compressive stresses of the chitosan scaffolds more remarkable than the pre-crosslinking procedure. The maximal compressive stress of the post-crosslinking c-CHITOSAN-50 scaffolds reached 6.21 ± 0.58 MPa, almost three times of that of the control scaffolds ($p < 0.001$). The reason might be also due to that the chitosan-rich domains are more compacted by the post-crosslinking method. UV-crosslinking also enhanced the equilibrium compressive stresses of the chitosan scaffolds, an indication of the viscous behavior of a material (Yousefi, Gauvin, Sun, DiRaddo, & Fernandes, 2007). The equilibrium stress of the post-crosslinking c-CHITOSAN-50 scaffolds (5.1 ± 0.32 MPa) was the highest among all the scaffolds, while the unmodified chitosan scaffolds possessed the lowest equilibrium stress (2.17 ± 0.19 MPa).

Our results indicate that the post-crosslinking process might be better for the fabrication of UV-crosslinked chitosan scaffolds compared with the pre-crosslinking method, due to larger

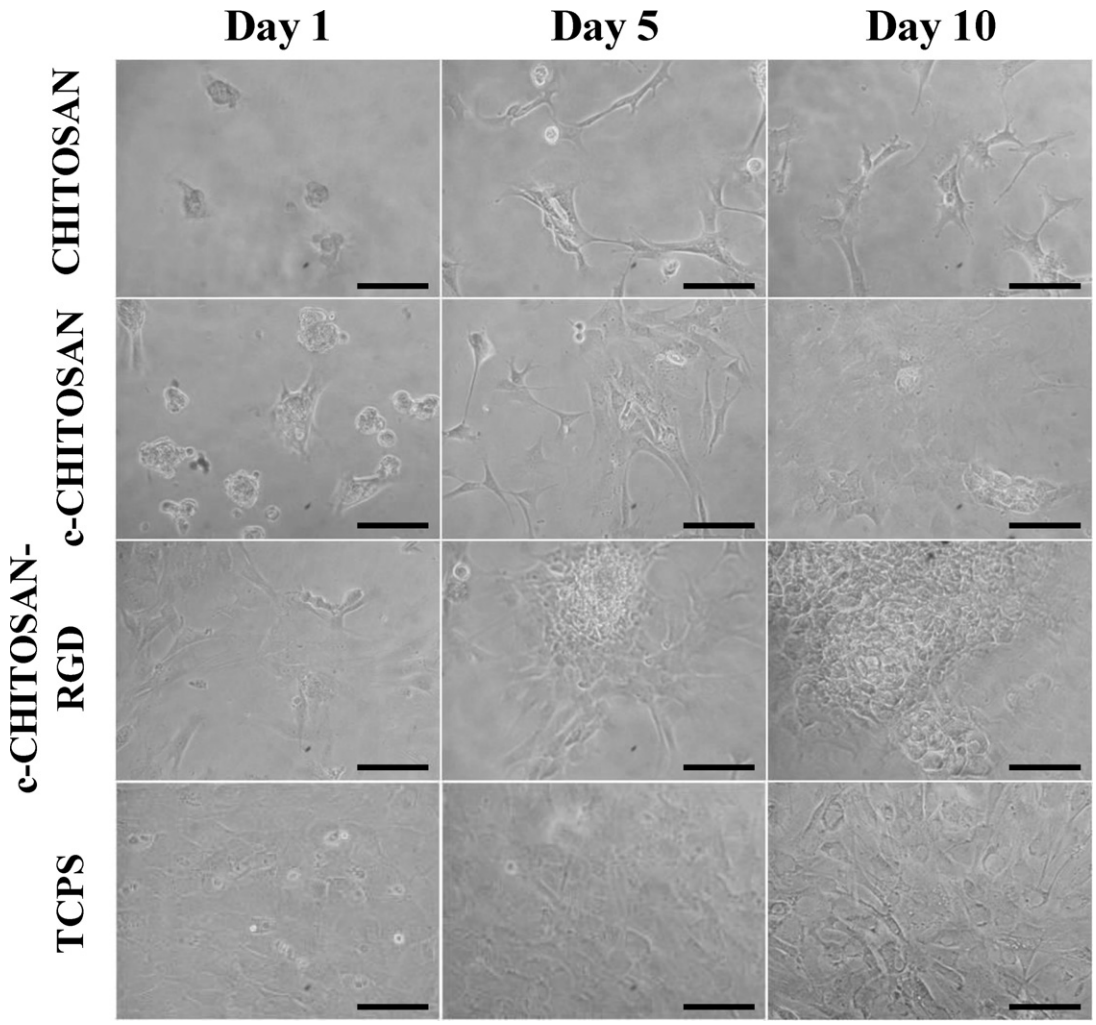

Fig. 3. The phase contrast microscopic images of the osteoblasts cultured on the different chitosan films for 1, 5 and 10 days (magnification 200×). The scale bars represent 100 μm.

pore sizes and better mechanical strength. Therefore, the post-crosslinking c-CHITOSAN-50 scaffold was chosen for fabrication of RGD-incorporated scaffolds for osteoblast culture and was designated as c-CHITOSAN in the rest of the text.

3.2. Osteoblast culture on the chitosan films

The impact of RGD-conjugation to the chitosan substrates on the attachment and proliferation of the osteoblasts were first evaluated on the two-dimensional chitosan films. Microscopic images showed that the primary osteoblasts attached poorly on the untreated chitosan films at Day 1, whereas more cells attached onto the c-CHITOSAN films (Fig. 3). On the other hand, the osteoblasts attached and spread well onto the c-CHITOSAN-RGD films. After 5 and 10 days of culture, the osteoblasts proliferated and spread on all types of the chitosan films, while cell clusters were found on the c-CHITOSAN-RGD films (Fig. 3).

The cell numbers on the chitosan films were further quantified (Fig. 4). Incorporation of RGD increased one-day cell attachment to 2.2×10^4 cells/cm^2, significantly higher than those on the unmodified chitosan and c-CHITOSAN films (1.2×10^4 and 1.4×10^4 cells/cm^2, respectively; $p < 0.05$). After 10 days of culture, the cell number on the c-CHITOSAN-RGD films was increased to 4.8×10^4 cells/cm^2, more than twice of that on the unmodified chitosan or c-CHITOSAN films ($\sim 2.3 \times 10^4$ cells/cm^2; $p < 0.001$). It is obvious that RGD incorporation efficiently enhanced the attachment and proliferation of the osteoblasts to the chitosan films. Therefore, we next studied the effects of RGD on bone tissue engineering in three-dimensional chitosan scaffolds.

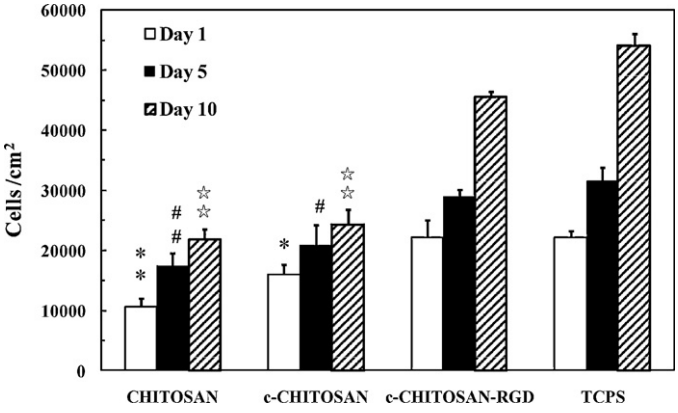

Fig. 4. The numbers of osteoblasts after 1, 5 and 10 days of culture on the CHITOSAN, c-CHITOSAN, and c-CHITOSAN-RGD films. Data are represented as mean ± standard deviation, $n = 4$. * and ** represent $p < 0.01$ and $p < 0.001$ vs. c-CHITOSAN-RGD on Day 1, respectively; # and ## represent $p < 0.01$ and $p < 0.001$ vs. c-CHITOSAN-RGD on Day 5, respectively; ☆☆ represents $p < 0.001$ vs. c-CHITOSAN-RGD on Day 10.

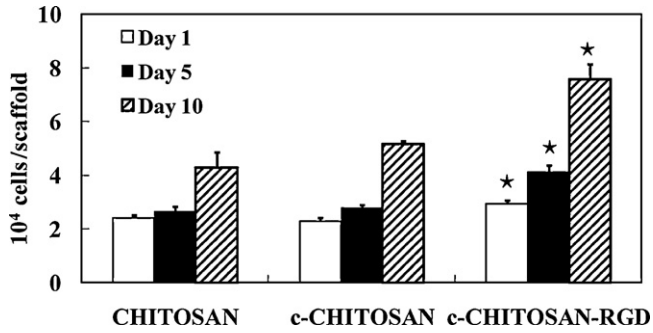

Fig. 5. The numbers of osteoblasts after 1, 5 and 10 days of culture in the CHITOSAN, c-CHITOSAN, and c-CHITOSAN-RGD scaffolds. Data are represented as mean ± standard deviation, $n = 4$. ⋆ $p < 0.001$ vs. CHITOSAN and c-CHITOSAN on the same day.

3.3. Osteoblast culture in the chitosan scaffolds

Initial attachment of the osteoblasts in the c-CHITOSAN-RGD scaffolds after one day culture (2.9×10^4 cells/scaffold) was only slightly higher than those on the unmodified chitosan and c-CHITOSAN scaffolds ($\sim 2.4 \times 10^4$ cells/scaffold) (Fig. 5, $p < 0.05$). Nevertheless, the osteoblasts grew much better in the c-CHITOSAN-RGD scaffolds compared with the unmodified chitosan and c-CHITOSAN scaffolds. After 10 days of culture, the osteoblasts cultured in the c-CHITOSAN-RGD scaffolds increased to 7.5×10^4 cells/scaffold, while the cell numbers in the other two types of scaffolds were less than 5×10^4 cells/scaffold ($p < 0.001$ vs. c-CHITOSAN-RGD). The doubling time of the osteoblasts in the c-CHITOSAN-RGD scaffolds was 6 days, in contrast to approximately 10 and 8 days in the unmodified chitosan and c-CHITOSAN scaffolds, respectively.

Calcium deposition in the chitosan scaffolds after 15 days of in vitro mineralization was stained by alizarin red and observed on the microscopic sections of the scaffolds. More red stains were observed on the c-CHITOSAN-RGD samples than the other two types of samples (Fig. 6), suggesting more calcium deposition by the osteoblasts cultured in the c-CHITOSAN-RGD scaffolds. Images E and F in Fig. 6, taken from the center of the c-CHITOSAN-RGD scaffolds, show that the osteoblasts penetrated into the c-CHITOSAN-RGD scaffolds and underwent mineralization at the center of the scaffolds. The calcium contents in the scaffolds were quantified after 3 weeks of mineralization culture. The total amount of calcium deposition in the unmodified chitosan and c-CHITOSAN scaffolds was about 732 ± 48 and 725 ± 30 μmole/scaffold ($p > 0.05$),

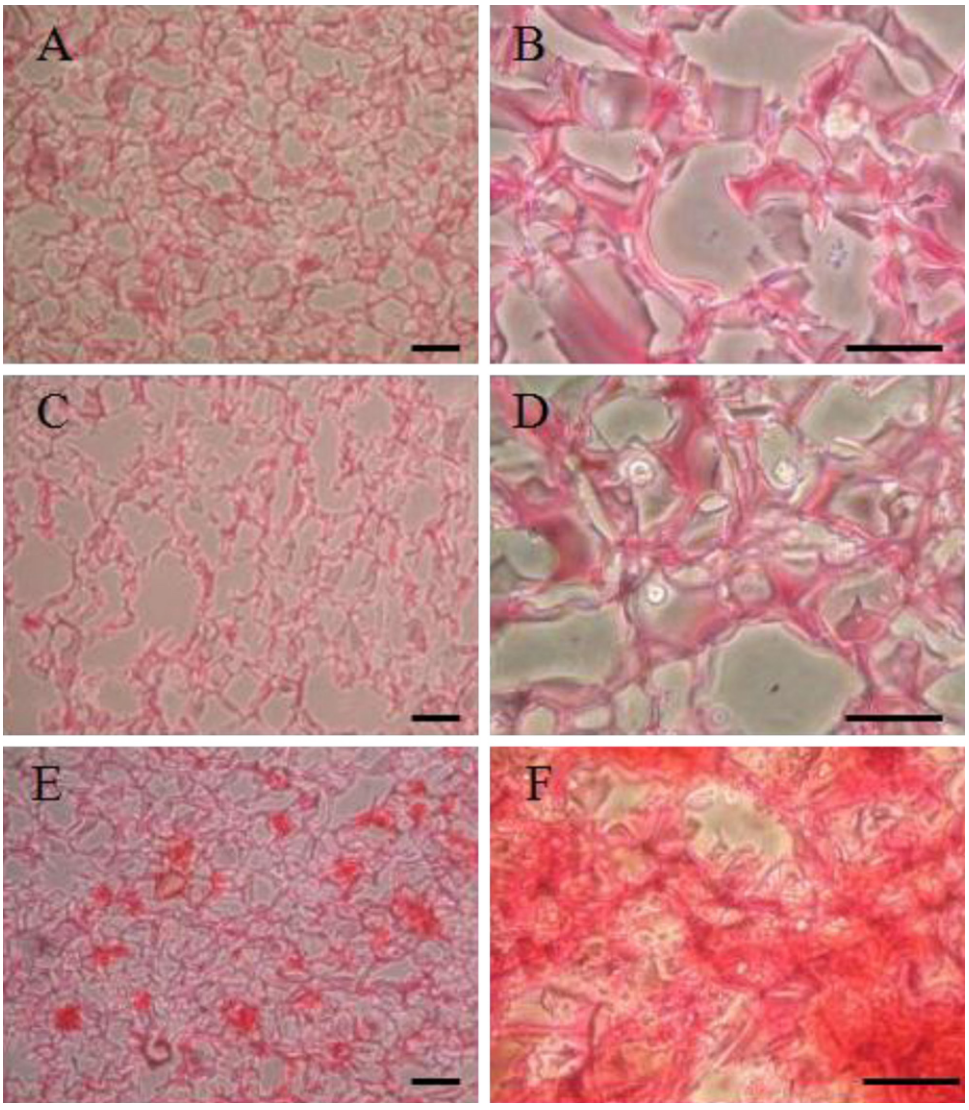

Fig. 6. The microscopic images of the sections of the osteoblast/scaffold constructs after 15 days of mineralization culture, and stained by alizarin red: CHITOSAN (A and B), c-CHITOSAN (C and D), and c-CHITOSAN-RGD (E and F). The magnification for (A), (C) and (E) was 100×, while that for (B), (D) and (F) was 200×. Scale bars = 100 μm.

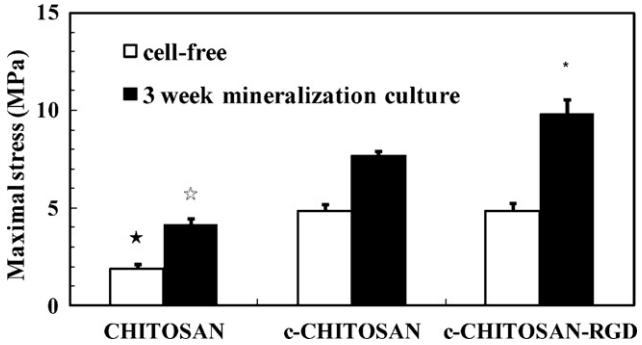

Fig. 7. The maximal stresses of the CHITOSAN, c-CHITOSAN and c-CHITOSAN-RGD scaffolds at 95% strain. Data are represented as mean ± standard deviation, $n = 4$. ⋆ $p < 0.001$ vs. the cell-free c-CHITOSAN and c-CHITOSAN-RGD; ☆ $p < 0.001$ vs. c-CHITOSAN and c-CHITOSAN-RGD after 3 weeks of mineralization; * $p < 0.001$ vs. c-CHITOSAN after 3 weeks of mineralization.

while that in the c-CHITOSAN-RGD scaffolds was greatly enhanced to ∼1400 ± 200 μmole/scaffold ($p < 0.001$ vs. CHITOSAN and c-CHITOSAN).

The compressive properties of the bone tissue engineered constructs after 3 weeks of mineralization culture were also analyzed. The compressive stress at 95% strain of the cell-free chitosan scaffolds was increased from 1.88 ± 0.344 MPa to 4.16 ± 0.322 MPa after cell culture (Fig. 7). The compressive stresses of the cell-free c-CHITOSAN and c-CHITOSAN-RGD scaffolds was similar (∼4.1 MPa), but after 3 weeks of mineralization culture, the mechanical properties were enhanced more in c-CHITOSAN-RGD than in c-CHITOSAN (9.81 ± 0.738 MPa and 7.68 ± 0.239 MPa, respectively, $p < 0.001$).

The strategy to fabricate RGD-bearing crosslinked chitosan scaffolds in this study is superior to the traditional approach. The commonly used strategy for RGD immobilization onto chitosan scaffolds is by post-conjugation, i.e. attaching RGD peptides onto pre-formed chitosan scaffolds via suitable chemical reactions (e.g. imide bond-forming reactions) to the amino or hydroxyl groups of chitosan molecules (Ho et al., 2005). Nevertheless, this strategy can neither control the density of RGD conjugation precisely nor guarantee uniform distribution of RGD peptides throughout the chitosan scaffolds. By our method, RGD peptides are first conjugated onto chitosan molecules prior to scaffold fabrication. Therefore, the RGD concentrations in scaffolds could be easily controlled by adjusting the amount of CHI-g-RGD. Furthermore, the post-conjugation of RGD may be limited by the diffusion of RGD peptides into tortuous porous structures of scaffolds, resulting in low RGD conjugation in the core of the scaffolds. Uneven distribution of RGD in scaffolds may deteriorate the functions of tissue engineered products. By our fabrication process, RGD could be homogeneously distributed throughout a scaffold if chitosan-g-RGD is well-mixed in the chitosan solution. As we expected, many osteoblasts grew into the center of the c-CHITOSAN-RGD scaffolds and deposited calcium minerals (Fig. 6), indicating that our RGD-conjugated chitosan scaffolds enhanced cellular penetration and functions inside the chitosan scaffolds.

4. Conclusion

In conclusion, we successfully developed a simple and reliable method to fabricate RGD-incorporated chitosan scaffolds with controllable mechanical properties. This technique can be applied not only to chitosan scaffolds but also to those based on other natural biomaterials such as proteins and polysaccharides. Furthermore, besides peptides, other types of bioactive molecules such as growth factors and drugs can be conjugated into a scaffold uniformly by our method. Besides scaffold fabrication, other forms of biomedical devices in the forms of films, beads and particles can be also fabricated. The extensive applicability of our technique should benefit various biomedical applications.

Acknowledgement

The authors gratefully acknowledge the financial support from National Science Council, Taiwan (Grant No.: 97-2628-E-002-028-MY2).

Appendix A. Supplementary data

Supplementary data associated with this article can be found, in the online version, at doi:10.1016/j.carbpol.2011.02.003.

References

Bakker, A., & Klein-Nulend, J. (2003). *Osteoblast isolation from murine calvariae and long bones* Totowa, NJ, USA: Humana Press.

Chung, T. W., Lu, Y. F., Wang, S. S., Lin, Y. S., & Chu, S. H. (2002). Growth of human endothelial cells on photochemically grafted Gly-Arg-Gly-Asp (GRGD) chitosans. *Biomaterials*, *23*(24), 4803–4809.

Das, M., & Fox, C. F. (1979). Chemical cross-linking in biology. *Annual Review of Biophysics and Bioengineering*, *8*, 165–193.

Fukuda, J., Khademhosseini, A., Yeo, Y., Yang, X., Yeh, J., Eng, G., et al. (2006). Micromolding of photocrosslinkable chitosan hydrogel for spheroid microarray and co-cultures. *Biomaterials*, *27*(30), 5259–5267.

Hacker, M., Tessmar, J., Neubauer, M., Blaimer, A., Blunk, T., Gopferich, A., et al. (2003). Towards biomimetic scaffolds: anhydrous scaffold fabrication from biodegradable amine-reactive diblock copolymers. *Biomaterials*, *24*(24), 4459–4473.

Hirai, A., Odani, H., & Nakajima, A. (1991). Determination of degree of deacetylation of chitosan by ^{1}H NMR spectroscopy. *Polymer Bulletin*, *26*, 87–94.

Ho, M. H., Kuo, P. Y., Hsieh, H. J., Hsien, T. Y., Hou, L. T., Lai, J. Y., et al. (2004). Preparation of porous scaffolds by using freeze-extraction and freeze-gelation methods. *Biomaterials*, *25*(1), 129–138.

Ho, M. H., Wang, D. M., Hsieh, H. J., Liu, H. C., Hsien, T. Y., Lai, J. Y., et al. (2005). Preparation and characterization of RGD-immobilized chitosan scaffolds. *Biomaterials*, *26*(16), 3197–3206.

Hoffmann, B., Seitz, D., Mencke, A., Kokott, A., & Ziegler, G. (2009). Glutaraldehyde and oxidised dextran as crosslinker reagents for chitosan-based scaffolds for cartilage tissue engineering. *Journal of Materials Science: Materials in Medicine*, *20*(7), 1495–1503.

Hsieh, C. Y., Tsai, S. P., Ho, M. H., Wang, D. M., Liu, C. E., Hsieh, C. H., et al. (2007). Analysis of freeze-gelation and cross-linking processes for preparing porous chitosan scaffolds. *Carbohydrate Polymers*, *67*(1), 124–132.

Huang, Y., Onyeri, S., Siewe, M., Moshfeghian, A., & Madihally, S. V. (2005). In vitro characterization of chitosan-gelatin scaffolds for tissue engineering. *Biomaterials*, *26*(36), 7616–7627.

Hynes, R. O. (1992). Integrins: versatility, modulation, and signaling in cell adhesion. *Cell*, *69*(1), 11–25.

Innocentini, M. D. M., Salvini, V. R., Pandolfelli, V. C., & Coury, J. R. (1999). Assessment of Forchheimer's equation to predict the permeability of ceramic foams. *Journal of the American Ceramic Society*, *82*(7), 1945–1948.

Ishihara, M., Nakanishi, K., Ono, K., Sato, M., Kikuchi, M., Saito, Y., et al. (2002). Photocrosslinkable chitosan as a dressing for wound occlusion and accelerator in healing process. *Biomaterials*, *23*(3), 833–840.

Karp, J. M., Yeo, Y., Geng, W., Cannizarro, C., Yan, K., Kohane, D. S., et al. (2006). A photolithographic method to create cellular micropatterns. *Biomaterials*, *27*(27), 4755–4764.

Kuo, Y. C., & Lin, C. Y. (2006). Effect of genipin-crosslinked chitin-chitosan scaffolds with hydroxyapatite modifications on the cultivation of bovine knee chondrocytes. *Biotechnology and Bioengineering*, *95*(1), 132–144.

Ling, K., Zheng, F., Li, J., Tang, R., Huang, J., Xu, Y., et al. (2008). Effects of substitution degree of photoreactive groups on the properties of UV-fabricated chitosan scaffold. *Journal of Biomedical Materials Research Part A*, *87*(1), 52–61.

Madihally, S. V., & Matthew, H. W. (1999). Porous chitosan scaffolds for tissue engineering. *Biomaterials*, *20*(12), 1133–1142.

Majima, T., Funakosi, T., Iwasaki, N., Yamane, S. T., Harada, K., Nonaka, S., et al. (2005). Alginate and chitosan polyion complex hybrid fibers for scaffolds in ligament and tendon tissue engineering. *Journal of Orthopaedic Science*, *10*(3), 302–307.

Massia, S. P., & Hubbell, J. A. (1990). Covalently attached GRGD on polymer surfaces promotes biospecific adhesion of mammalian cells. *Annals of the New York Academy of Sciences*, *589*, 261–270.

Muzzarelli, R. A. A. (2009a). Chitins and chitosans for the repair of wounded skin, nerve, cartilage and bone. *Carbohydrate Polymers*, *76*, 167–182.

Muzzarelli, R. A. A. (2009b). Genipin-crosslinked chitosan hydrogels as biomedical and pharmaceutical aids. *Carbohydrate Polymers*, *77*, 1–9.

Muzzarelli, R. A. A. (2011). Chitosan composites with inorganics, morphogenetic proteins and stem cells, for bone regeneration. *Carbohydrate Polymers*, *83*(4), 1433–1445.

Obara, K., Ishihara, M., Ishizuka, T., Fujita, M., Ozeki, Y., Maehara, T., et al. (2003). Photocrosslinkable chitosan hydrogel containing fibroblast growth factor-2 stimulates wound healing in healing-impaired db/db mice. *Biomaterials*, *24*(20), 3437–3444.

Ono, K., Saito, Y., Yura, H., Ishikawa, K., Kurita, A., Akaike, T., et al. (2000). Photocrosslinkable chitosan as a biological adhesive. *Journal of Biomedical Materials Research*, *49*(2), 289–295.

Ruoslahti, E., & Pierschbacher, M. D. (1987). New perspectives in cell adhesion: RGD and integrins. *Science*, *238*(4826), 491–497.

Tsai, W. B., Chen, R. P., Wei, K. L., Chen, Y. R., Liao, T. Y., Liu, H. L., et al. (2009). Polyelectrolyte multilayer films functionalized with peptides for promoting osteoblast functions. *Acta Biomaterialia*, *5*(9), 3467–3477.

Tsai, W. B., Chen, R. P., Wei, K. L., Tan, S. F., & Lai, J. Y. (2010). Modulation of RGD-functionalized polyelectrolyte multilayer membranes for promoting osteoblast function. *Journal of Biomaterials Science. Polymer Edition*, *21*(3), 377–394.

Tsai, W. B., Shi, Q., Grunkemeier, J. M., McFarland, C., & Horbett, T. A. (2004). Platelet adhesion to radiofrequency glow-discharge-deposited fluorocarbon polymers preadsorbed with selectively depleted plasmas show the primary role of fibrinogen. *Journal of Biomaterials Science. Polymer Edition*, *15*(7), 817–840.

VandeVord, P. J., Matthew, H. W., DeSilva, S. P., Mayton, L., Wu, B., & Wooley, P. H. (2002). Evaluation of the biocompatibility of a chitosan scaffold in mice. *Journal of Biomedical Materials Research*, *59*(3), 585–590.

Wang, P. Y., Chow, H. H., Lai, J. Y., Liu, H. L., & Tsai, W. B. (2009). Dynamic compression modulates chondrocyte proliferation and matrix biosynthesis in chitosan/gelatin scaffolds. *Journal of Biomedical Materials Research Part B: Applied Biomaterials*, *91*(1), 143–152.

Yousefi, A. M., Gauvin, C., Sun, L., DiRaddo, R. W., & Fernandes, J. (2007). Design and fabrication of 3D-plotted polymeric scaffolds in functional tissue engineering. *Polymer Engineering and Science*, *47*(5), 608–618.